Theoretical and Numerical Foundations for the Use of Micro-Columns as Angular Motion Sensors

Matthew J. Zahr
Professor Sanjay Govindjee
University of California, Berkeley

July 28, 2014

Abstract

This work presents a model for the use of an ensemble of microcolumns as angular motion sensors. The methodology for angular detection is most suitable for small, high-frequency systems. This project makes use of the Equipartition Theorem and the Louisville Equation to determine the evolution of the probability density distribution of the location of the microcolumn tips. The work formulates the problem of interest, establishes a theoretical and computational model, presents the numerical stability analysis, and the simulation results. The Two-Step Lax Wendroff method was the explicit integration scheme used.

1 Introduction

This document investigates a methodology for detecting angular motion that has not been previously considered. The detection of angular motion is a fundamental topic and therefore the applications are seemingly endless. Applications that rely on angular motion detection have great variability in their size scale and frequency scale. The size scale of can vary from planets (10^6 m) to smartphones (10^{-2} m), a magnitude range of 10^8 m; while the frequency scale can vary from the revolution of a planet about the sun (10^{-8} Hz) to the frequency of a clock signal in modern computers (10^9 Hz), a magnitude range of 10^{17} Hz. The technique developed in this document is most suitable for small, high-frequency systems.

2 Problem Formulation

The model considered is an ensemble of identical microcolumns fixed on a plate that rotates about an axis though the center of its broad face. By an ensemble, we are referring to an idealization consisting of a large number of members that comprise a system, thereby validating the use of a statistical model. Due to the Equipartition Theorem, even when the angular velocity of the plate is zero, the columns have kinetic energy, which translates into dectectable motion given the size of the members. On average, the envelope of the motion of each column will be elliptical with the direction and magnitude of the major and minor axes dependent on the minimum and maximum bending stiffness, respectively. If the base is rotated with angular velocity $\dot{\theta}$, an observer *fixed on the base* will, on average, see the ellipse envelope rotate. Quantification of the rotation of the ellipse relative to an observer fixed on the plate will enable us to solve an inverse problem to determine the angular motion of the plate. Note that this analysis is valid since we have an ensemble of microcolumns, therefore, by averaging over the ensemble we can determine the behavior of the ellipse on average. Thus, if we consider a probability density distribution that describes the location of the tip of some microcolumn, we would expect the same behavior, on average.

Each microcolumn is approximated as a lumped mass attached to springs of stiffness equal to the bending stiffness of the microcolumn in each direction. With the physical model established, we now consider the mathematical model and subsequently, the numerical analysis. The physical setup of the problem is presented in Fig. 1.

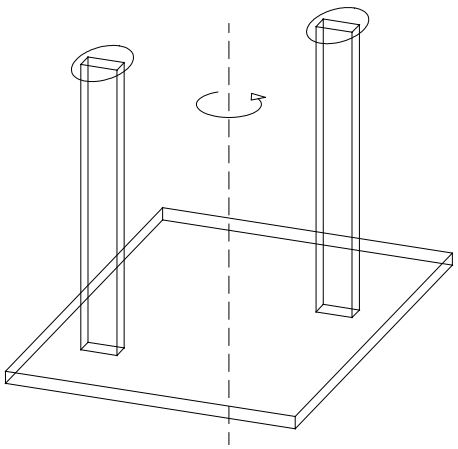

Figure 1: Physical setup of microcolumn ensemble on rotating plate, with the ellipse defining their respective displacement envelopes.

3 Mathematical Model

The system described in Sec. 2 is governed by the Louisville Equation:

$$\frac{\partial \rho}{\partial t} = -\left[\frac{\partial \rho}{\partial \mathbf{x}} \cdot \frac{\partial H}{\partial \mathbf{p}} - \frac{\partial \rho}{\partial \mathbf{p}} \cdot \frac{\partial H}{\partial \mathbf{x}}\right], \tag{1}$$

where $\rho = \rho(\mathbf{x}; \dot{\mathbf{x}}; t) \in \mathbb{R}^+$ is the probability density describing the likelihood of the tip of a microcolumn in the ensemble being located at position $\mathbf{x}$ with velocity $\dot{\mathbf{x}}$. The momentum of a microcolumn in the ensemble is $\mathbf{p} = m\dot{\mathbf{x}}$, with mass m. It is important to note that the positions, $\mathbf{x}$, and velocities, $\dot{\mathbf{x}}$, are measured relative to an inertial reference frame.

As mentioned in Sec. 1, the applications of the model presented in this document concern the evolution of the probability density function with respect to a *rotating coordinate system* fixed on the base plate. Therefore, it is necessary to reformulate (1) in terms of positions and velocities in a rotating reference frame. Let

$$\mathbf{x} = \begin{bmatrix} x_1 \\ x_2 \end{bmatrix} \qquad \text{and} \qquad \mathbb{X} = \begin{bmatrix} X_1 \\ X_2 \end{bmatrix}$$

denote the inertial and rotating reference frames, respectively. The inertial and rotating frames are related according to

$$\mathbb{X} = \mathbf{R}^T\mathbf{x} \qquad \text{and} \qquad \mathbf{x} = \mathbf{R}\mathbb{X} \tag{2}$$

and differentiation of these equation with respect to time yields

$$\dot{\mathbb{X}} = \dot{\mathbf{R}}^T\mathbf{x} + \mathbf{R}^T\dot{\mathbf{x}} \qquad \text{and} \qquad \dot{\mathbf{x}} = \dot{\mathbf{R}}\mathbb{X} + \mathbf{R}\dot{\mathbb{X}}, \tag{3}$$

repectively, where

$$\mathbf{R} = \begin{bmatrix} \cos\theta & -\sin\theta \\ \sin\theta & \cos\theta \end{bmatrix}$$

is the rotation matrix of the system. The following are useful relationships that follow from the above formulation

$$\mathbf{R}\mathbf{R}^T = \mathbf{I}_{2\times 2} \qquad \mathbf{R}^T\dot{\mathbf{R}} = \begin{bmatrix} 0 & -\dot{\theta} \\ \dot{\theta} & 0 \end{bmatrix} \qquad \dot{\mathbf{R}}^T\mathbf{R} = \begin{bmatrix} 0 & \dot{\theta} \\ -\dot{\theta} & 0 \end{bmatrix} \qquad \dot{\mathbf{R}}\dot{\mathbf{R}}^T = \dot{\theta}^2\mathbf{I}_{2\times 2} \tag{4}$$

and

$$\frac{\partial \mathbb{X}}{\partial \mathbf{x}} = \mathbf{R}^T \qquad \frac{\partial \mathbb{X}}{\partial \dot{\mathbf{x}}} = 0 \qquad \frac{\partial \dot{\mathbb{X}}}{\partial \mathbf{x}} = \dot{\mathbf{R}}^T \qquad \frac{\partial \dot{\mathbb{X}}}{\partial \dot{\mathbf{x}}} = \mathbf{R}^T, \tag{5}$$

where $\mathbf{I}_{2\times 2}$ is the 2×2 identity matrix.

By approximating our system of columns as a system of lumped masses and springs, the hamiltonian of the system is found to be

$$H = \frac{1}{2m}\mathbf{p}\cdot\mathbf{p} + \frac{1}{2}\mathbf{x}\cdot\mathbf{R}\mathbf{K}\mathbf{R}^T\mathbf{x},$$

where $\mathbf{K} \in \mathbb{R}^{2\times 2}$ is the stiffness matrix of the columns in the ensemble.

Partial differentiation of the hamiltonian of the system with respect to $\mathbf{x}$ and $\mathbf{p}$ and substituting (2) and (3) into the result yields

$$\frac{\partial H}{\partial \mathbf{x}} = \mathbf{R}\mathbf{K}\mathbf{R}^T\mathbf{x} = \mathbf{R}\mathbf{K}\mathbf{R}^T\mathbf{R}\mathbb{X} = \mathbf{R}\mathbf{K}\mathbb{X} \tag{6}$$

$$\frac{\partial H}{\partial \mathbf{p}} = \frac{\mathbf{p}}{m} = \dot{\mathbf{x}} = \dot{\mathbf{R}}\mathbb{X} + \mathbf{R}\dot{\mathbb{X}}. \tag{7}$$

Consider now the reformulation of ρ as $\rho = \rho(\mathbb{X}(\mathbf{x},\dot{\mathbf{x}}), \dot{\mathbb{X}}(\mathbf{x},\dot{\mathbf{x}}))$. Differentiation of ρ with respect to the inertial frame phase coordinates and appropriate application of the chain rule of differentiation produces a relation between the partial derivatives of ρ with respect to the two coordinate systems. Substituting (5) into this relation yields

$$\frac{\partial \rho}{\partial \mathbf{x}} = \left(\frac{\partial \mathbb{X}}{\partial \mathbf{x}}\right)^T \frac{\partial \rho}{\partial \mathbb{X}} + \left(\frac{\partial \dot{\mathbb{X}}}{\partial \mathbf{x}}\right)^T \frac{\partial \rho}{\partial \dot{\mathbb{X}}} = \mathbf{R}\frac{\partial \rho}{\partial \mathbb{X}} + \dot{\mathbf{R}}\frac{\partial \rho}{\partial \dot{\mathbb{X}}} \tag{8}$$

$$\frac{\partial \rho}{\partial \mathbf{p}} = \frac{\partial \rho}{\partial (m\dot{\mathbf{x}})} = \frac{1}{m}\frac{\partial \rho}{\partial \dot{\mathbf{x}}} = \frac{1}{m}\left[\left(\frac{\partial \mathbb{X}}{\partial \dot{\mathbf{x}}}\right)^T \frac{\partial \rho}{\partial \mathbb{X}} + \left(\frac{\partial \dot{\mathbb{X}}}{\partial \dot{\mathbf{x}}}\right)^T \frac{\partial \rho}{\partial \dot{\mathbb{X}}}\right] = \frac{1}{m}\mathbf{R}\frac{\partial \rho}{\partial \dot{X}}. \tag{9}$$

Notice that with (6) - (9), we have reformulated every term in (1) in the rotating reference frame. Thus, by substituting (6) - (9) into (1), we have:

$$\begin{aligned}
\frac{\partial \rho}{\partial t} &= -\left[\left(\mathbf{R}\frac{\partial \rho}{\partial \mathbb{X}} + \dot{\mathbf{R}}\frac{\partial \rho}{\partial \dot{\mathbb{X}}}\right)\cdot(\dot{\mathbf{R}}\mathbb{X} + \mathbf{R}\dot{\mathbb{X}}) - \frac{1}{m}\mathbf{R}\frac{\partial \rho}{\partial \dot{\mathbb{X}}}\cdot\mathbf{R}\mathbf{K}\mathbb{X}\right] \\
&= -\left[\left(\left(\frac{\partial \rho}{\partial \mathbb{X}}\right)^T\mathbf{R}^T + \left(\frac{\partial \rho}{\partial \dot{\mathbb{X}}}\right)^T\dot{\mathbf{R}}^T\right)(\dot{\mathbf{R}}\mathbb{X} + \mathbf{R}\dot{\mathbb{X}}) - \frac{1}{m}\left(\frac{\partial \rho}{\partial \dot{\mathbb{X}}}\right)^T\mathbf{R}^T\mathbf{R}\mathbf{K}\mathbb{X}\right] \\
&= -\left[\left(\frac{\partial \rho}{\partial \mathbb{X}}\right)^T\left(\mathbf{R}^T\dot{\mathbf{R}}\mathbb{X} + \mathbf{R}^T\mathbf{R}\dot{\mathbb{X}}\right) + \left(\frac{\partial \rho}{\partial \dot{\mathbb{X}}}\right)^T\left(\dot{\mathbf{R}}^T\dot{\mathbf{R}}\mathbb{X} + \dot{\mathbf{R}}^T\mathbf{R}\dot{\mathbb{X}}\right) - \frac{1}{m}\left(\frac{\partial \rho}{\partial \dot{\mathbb{X}}}\right)^T\mathbf{K}\mathbb{X}\right] \\
&= -\left[\frac{\partial \rho}{\partial \mathbb{X}}\cdot\left(\mathbf{R}^T\dot{\mathbf{R}}\mathbb{X} + \dot{\mathbb{X}}\right) + \frac{\partial \rho}{\partial \dot{\mathbb{X}}}\cdot\left(\dot{\theta}^2\mathbb{X} + \dot{\mathbf{R}}^T\mathbf{R}\dot{\mathbb{X}} - \frac{1}{m}\mathbf{K}\mathbb{X}\right)\right].
\end{aligned}$$

Hence, the governing equation for the problem of interest in the rotating coordinate system is

$$\frac{\partial \rho}{\partial t} = -\left[\frac{\partial \rho}{\partial \mathbb{X}}\cdot\left(\mathbf{R}^T\dot{\mathbf{R}}\mathbb{X} + \dot{\mathbb{X}}\right) + \frac{\partial \rho}{\partial \dot{\mathbb{X}}}\cdot\left(\dot{\theta}^2\mathbb{X} + \dot{\mathbf{R}}^T\mathbf{R}\dot{\mathbb{X}} - \frac{1}{m}\mathbf{K}\mathbb{X}\right)\right]. \tag{10}$$

3.1 Collision Term

Since (10) is idealistic in the sense that it is entirely non-dissipative, we need to incorporate damping effects into the system for practical purposes. To introduce damping effects that are always present due to collisions of particles in the atmosphere with the microcolumns, we include a first order approximation, dubbed the collision term, ϕ, where

$$\phi(\rho, \rho_0, \tau) = \frac{\rho_0 - \rho(t)}{\tau},$$

where ρ_0 is the equilibrium probability density distribution and $\tau \in \mathbb{R}^+$ is the relaxation time. Notice that the collision term can be viewed as a vector in state space that is directed from $\rho(t)$ toward ρ_0. This is a useful interpretation in that it suggests that the collision term forces the system toward equilibrium.

Therefore, (10) becomes

$$\boxed{\frac{\partial \rho}{\partial t} = -\left[\frac{\partial \rho}{\partial \mathbb{X}} \cdot \left(\mathbf{R}^T \dot{\mathbf{R}} \mathbb{X} + \dot{\mathbb{X}}\right) + \frac{\partial \rho}{\partial \dot{\mathbb{X}}} \cdot \left(\dot{\theta}^2 \mathbb{X} + \dot{\mathbf{R}}^T \mathbf{R} \dot{\mathbb{X}} - \frac{1}{m} \mathbf{K} \mathbb{X}\right)\right] + \phi(\rho, \rho_0, \tau).} \tag{11}$$

4 Numerical Analysis

4.1 Integration Scheme

The integration scheme scheme selected to numerically solve (1) is known as the Two Step Lax-Wendroff (TSLW) method, initially developed in [1] and modified in [2]. The modified version in [2] was used in this document. The TSLW method is an explicit integration scheme tailored for hyperbolic partial differential equations. This integration scheme was selected for the following reasons: 1) due to the physics of the problem, it was necessary to use a non-dissipative integration scheme, 2) the dimensionality of the problem suggests that implicit integration would be computationally too expensive, and 3) the TSLW method has enhanced stability properties over the traditional Forward Euler scheme, necessary for hyperbolic PDEs. The TSLW method can be applied to the following hyperbolic system of equations:

$$\frac{\partial W}{\partial t} = \frac{\partial [A(W)]}{\partial x_1} + \frac{\partial [B(W)]}{\partial x_2} + \frac{\partial [C(W)]}{\partial x_3} + \frac{\partial [D(W)]}{\partial x_4}, \tag{12}$$

where $x_i \in [a_i, b_i]$, for $i \in \{1, 2, 3, 4\}$ are the spatial coordinates of the problem, t is the temporal variable, W is the unknown variable, and A, B, C, D are functions of W (nonlinear in general).

Both steps of the TSLW method are outlined below. The subscripts define the spatial coordinate, the superscripts define the temporal coordinate, and Δx_i is the grid spacing in the x_i-dimension for $i \in \{1, 2, 3, 4\}$. In the first step, an "intermediate" grid of values is computed at a half time step via averaging of the values of W on the corners of the hyper-cubes in $\mathbb{R}^4$ that define the cells of the four dimensional grid and the averaging of the partial derivatives of A, B, C, D with respect to the x_1, x_2, x_3, x_4 directions, respectively, across these hyper-cubes. The second step uses the "intermediate" grid to compute the values of W on the original grid to complete the full time step.

$$\begin{aligned}
W^{n+1/2}_{i+1/2,j+1/2,k+1/2,l+1/2} = \; & < W^n_{i,j,k,l} >_{16} + \frac{\Delta t}{2\Delta x_1}(< W^n(x_1 = i+1) >^1_8 - < W^n(x_1 = i) >^1_8) \\
& + \frac{\Delta t}{2\Delta x_2}(< W^n(x_2 = j+1) >^2_8 - < W^n(x_2 = j) >^2_8) \\
& + \frac{\Delta t}{2\Delta x_3}(< W^n(x_3 = k+1) >^3_8 - < W^n(x_3 = k) >^3_8) \\
& + \frac{\Delta t}{2\Delta x_4}(< W^n(x_4 = l+1) >^4_8 - < W^n(x_4 = l) >^4_8) \\
W^{n+1}_{i,j,k,l} = \; & W^n_{i,j,k,l} + \frac{\Delta t}{\Delta x_1}(< W^n(x_1 = i + \tfrac{1}{2}) >^1_8 - < W^n(x_1 = i - \tfrac{1}{2}) >^1_8) \\
& + \frac{\Delta t}{\Delta x_2}(< W^n(x_2 = j + \tfrac{1}{2}) >^2_8 - < W^n(x_2 = j - \tfrac{1}{2} >^2_8) \\
& + \frac{\Delta t}{\Delta x_3}(< W^n(x_3 = k + \tfrac{1}{2}) >^3_8 - < W^n(x_3 = k - \tfrac{1}{2}) >^3_8) \\
& + \frac{\Delta t}{\Delta x_4}(< W^n(x_4 = l + \tfrac{1}{2}) >^4_8 - < W^n(x_4 = l - \tfrac{1}{2}) >^4_8),
\end{aligned}$$

where

$< \cdot >_{16}$ = average of $(\cdot)$ using the 16 "corner" grid points

$< \cdot() >^\kappa_8$ = average of $(\cdot)$ using the 8 grid points while holding coordinate κ fixed at the point specified inside ().

Notice that the collision term in (11) does not involve partial derivatives of ρ. Therefore, this term will be dealt with separately. Expansion of the dot products and matrix multiplication involving the rotation matrices in (10), with the aid of the relations in (4), yields the following equation

$$\frac{\partial \rho}{\partial t} = -\left[\frac{\partial \rho}{\partial X_1}(-X_2\dot{\theta} + \dot{X}_1) + \frac{\partial \rho}{\partial X_2}(X_1\dot{\theta} + \dot{X}_2) + \frac{\partial \rho}{\partial \dot{X}_1}(X_1(\dot{\theta}^2 - \frac{k_{11}}{m}) + \dot{X}_2\dot{\theta}) + \frac{\partial \rho}{\partial \dot{X}_2}(X_2(\dot{\theta}^2 - \frac{k_{22}}{m}) - \dot{X}_1\dot{\theta})\right]. \tag{13}$$

Now, let us introduce some notation: $X_1 \to 1$, $X_2 \to 2$, $\dot{X}_1 \to 3$, $\dot{X}_2 \to 4$ and let

$$\begin{aligned} f_1 &= -(-X_2\dot{\theta} + \dot{X}_1) \\ f_2 &= -(X_1\dot{\theta} + \dot{X}_2) \\ f_3 &= -(X_1(\dot{\theta}^2 - \frac{k_{11}}{m}) + \dot{X}_2\dot{\theta}) \\ f_4 &= -(X_2(\dot{\theta}^2 - \frac{k_{22}}{m}) - \dot{X}_1\dot{\theta}) \end{aligned}$$

Substitution of this notation into (13) produces a linear partial differential equation in the form of (12) with $W = \rho$, $A(\rho) = f_1\rho$, $B(\rho) = f_2\rho$, $C(\rho) = f_3\rho$, and $D(\rho) = f_4\rho$.

$$\frac{\partial \rho}{\partial t} = \frac{\partial \rho}{\partial \mathbb{X}_1} f_1 + \frac{\partial \rho}{\partial \mathbb{X}_2} f_2 + \frac{\partial \rho}{\partial \dot{\mathbb{X}}_1} f_3 + \frac{\partial \rho}{\partial \dot{\mathbb{X}}_2} f_4 \tag{14}$$

Finally, application of the TSLW method to (14) yields the following discretization. MATLAB was used to perform the computations.

$$\begin{aligned} \rho^{n+1/2}_{i+1/2,j+1/2,k+1/2,l+1/2} =& < \rho^n_{i,j,k,l} >_{16} + \frac{\Delta t}{2\Delta X_1} < f^n_1 >_{16} (< \rho^n(X_1 = i+1) >^1_8 - < \rho^n(X_1 = i) >^1_8) \\ &+ \frac{\Delta t}{2\Delta X_2} < f^n_2 >_{16} (< \rho^n(X_2 = j+1) >^2_8 - < \rho^n(X_2 = j) >^2_8) \\ &+ \frac{\Delta t}{2\Delta \dot{X}_1} < f^n_3 >_{16} (< \rho^n(\dot{X}_1 = k+1) >^3_8 - < \rho^n(\dot{X}_1 = k) >^3_8) \\ &+ \frac{\Delta t}{2\Delta \dot{X}_2} < f^n_4 >_{16} (< \rho^n(\dot{X}_2 = l+1) >^4_8 - < \rho^n(\dot{X}_2 = l) >^4_8) \end{aligned}$$

$$\begin{aligned} \rho^{n+1}_{i,j,k,l} =& \rho^n_{i,j,k,l} + \frac{\Delta t}{\Delta X_1} < f^n_1 >_{16} (< \rho^n(X_1 = i + \tfrac{1}{2}) >^1_8 - < \rho^n(X_1 = i - \tfrac{1}{2}) >^1_8) \\ &+ \frac{\Delta t}{\Delta X_2} < f^n_2 >_{16} (< \rho^n(X_2 = j + \tfrac{1}{2}) >^2_8 - < \rho^n(X_2 = j - \tfrac{1}{2} >^2_8) \\ &+ \frac{\Delta t}{\Delta \dot{X}_1} < f^n_3 >_{16} (< \rho^n(\dot{X}_1 = k + \tfrac{1}{2}) >^3_8 - < \rho^n(\dot{X}_1 = k - \tfrac{1}{2}) >^3_8) \\ &+ \frac{\Delta t}{\Delta \dot{X}_2} < f^n_4 >_{16} (< \rho^n(\dot{X}_2 = l + \tfrac{1}{2}) >^4_8 - < \rho^n(\dot{X}_2 = l - \tfrac{1}{2}) >^4_8) \end{aligned}$$

At this point, the collision term is incorporated to the system as follows:

$$\rho^{n+1}_{i,j,k,l} = \rho^{n+1}_{i,j,k,l} + \frac{\rho_0 - \rho^{n+1}_{i,j,k,l}}{\tau}.$$

This marks the completion of a single time step. Repeat as necessary to advance the solution in time.

4.2 Stability Analysis

A von Neumann stability analysis was used to determine the regions of stability for the TSLW method on (1). The stability analysis was performed as follows:

- Assume
$$\rho^n_{j,k,l,m} = \zeta^n e^{i(\alpha j + \beta k + \gamma m + \kappa m)}, \tag{15}$$
where ζ is constant, $i = \sqrt{-1}$, and $\alpha, \beta, \gamma, \kappa \in \mathbb{R}$. Notice that this is a single term of the Fourier series representation for $\rho^n_{i,j,k,l}$.

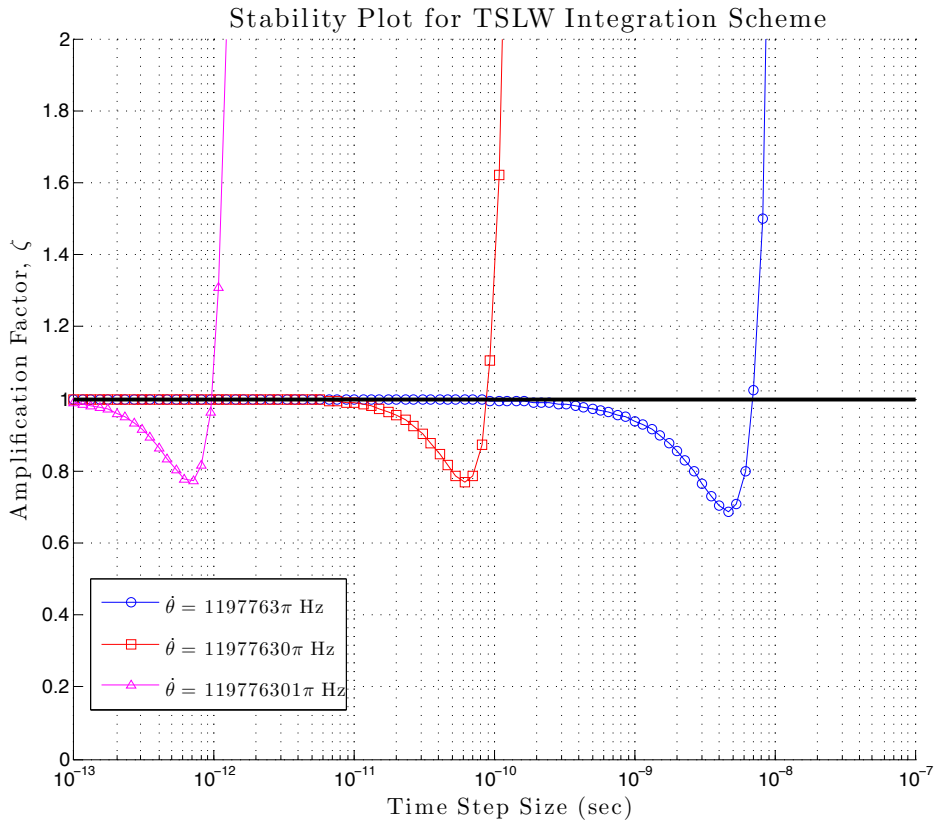

Figure 2: Sample Stability Plot for Three Different Angular Velocities for the TSLW Integration Scheme

- Insert into the TSLW integration equations to get the following expression:

$$\rho_{j,k,l,m}^{n+1} = \zeta^n e^{i(\alpha j+\beta k+\gamma m+\kappa m)} \Psi(\alpha, \beta, \gamma, \kappa) \tag{16}$$

- Equate (15) with $n = n + 1$ and (16) to find:

$$\zeta = \Psi(\alpha, \beta, \gamma, \kappa) \tag{17}$$

- To ensure the solution remains stable for all time, we require

$$|\zeta| = |\Psi(\alpha, \beta, \gamma, \kappa)| \leq 1 \tag{18}$$

Since the problem of interest has four "spatial" dimensions and the integration scheme requires multiple steps, the algebra involved quickly becomes intractable. Therefore, the details of the computations were carried out using the symbolic editor in MATLAB. The resulting expression is quite lengthy, so the stability analysis is contained in a numerical tool that can be used to generate plots that illustrate the regions of admissible time increments for stable solutions. An example of such a plot is shown in Fig. 2 for three different values of $\dot{\theta}$. The permissible time step sizes are those such that the amplification factor, ζ, is less than unity. Notice that as $\dot{\theta}$ increases by an order of magnitude, the time step must decrease by two orders of magnitude to maintain stability. This can be explained by the presence of a $\dot{\theta}^2$ term in (10).

5 Numerical Experiment: System Dynamics

In this section, a numerical experiment is conducted whereby the system dynamics described in this document are analyzed. The following parameters of a representative micro-column and the base plate were used in the numerical experiment:

- Cross-section width: $b = 20$ nm
- Cross-section height: $h = 40$ nm
- Length of column: $L = 10$ μm
- Young's Modulus of Material: $E = 800$ GPa
- Material Density: $\varrho = 2260$ $\frac{\text{kg}}{\text{m}^3}$
- Ambient Temperature: $T = 300$ K
- Boltzmann's Constant: $k_b = 1.3806503 \times 10^{-23}$ $\frac{\text{J}}{\text{K}}$
- Relaxation Time: $\tau = 1000$ sec

From these parameters, we have the following computed quantities:

- Column mass: $m = \varrho bhl$
- Moment of Inertia about Strong Axis: $I_{xx} = \frac{1}{12}bh^3 = 1.067 \times 10^{-31}$ m^4
- Moment of Inertia about Weak Axis: $I_{yy} = \frac{1}{12}b^3h = 2.667 \times 10^{-32}$ m^4
- Bending Stiffness about Weak Axis : $k_{11} = \frac{3EI_{yy}}{L^3} = 6.4 \times 10^{-5}$ $\frac{\text{N}}{\text{m}}$
- Bending Stiffness about Strong Axis: $k_{22} = \frac{3EI_{xx}}{L^3} = 2.56 \times 10^{-4}$ $\frac{\text{N}}{\text{m}}$
- Natural Frequency of Bending about the Weak Axis: $\Omega_1 = \sqrt{\frac{k_{11}}{m}} = 5.9888\pi \times 10^5$ Hz
- Natural Frequency of Bending about the Strong Axis: $\Omega_2 = \sqrt{\frac{k_{22}}{m}} = 1.1978\pi \times 10^6$ Hz

Finally, the angular motion function of the plate that was investigated in this document is:

$$\dot{\theta}(t) = \max\{\Omega_1, \Omega_2\}[H(t) - H(t - 4.0 \times 10^{-7})]$$

$$t \in [0, 1 \times 10^{-6}]\text{sec}$$

$$\Delta t = 1 \times 10^{-9}\text{sec}$$

Notice that in this case $\max\{\Omega_1, \Omega_2\} = \Omega_2 = 1.1978\pi \times 10^6$ Hz is the natural frequency of the columns about the strong axis. Therefore, one wold expect amplified displacements about the strong axis, which will translate into amplified displacements about both axes due to the rotation of the plate. From these parameters, a simulation of the probability distribution of the microcolumn location was executed (with constant time step Δt) and the results are presented in Figs. 3 and 4.

Figure 3 presents the contour snapshots of the probability density distribution at specific times in the time interval. The top left corner is the equilibrium position of the probability density distribution (i.e. if the base was fixed). As the base begins to rotate at $t = 0$, the ellipse defining the probability density distribution of the location of the cantilever tip begins to rotate relative to an observer on the plate. Another phenomena that occurs during the rotation is a "spreading out" of the probability density distribution. Physically, the rotation of the base translates into amplified deflections of the microcolumns, making the probability density shift outwards (i.e. it becomes more likely to see the column tip farther away from the ellipse center). The outward shift corresponds to a decrease in the values of the probability density nearly the ellipse center since the probability density distribution must always integrate to unity. This can be seen in the plot as a widening in the gap between contour lines. At $t = 4 \times 10^{-7}$ sec, the base is abruptly brought to a stop, at which point the ellipse reaches it maximal angle of rotation. Due to the collision term, the ellipse begins to rotate back toward equilibrium and the coutour lines become closer. This corresponds to an inward shift of the probability density distribution (the argument is exactly the reverse of that given above). At $t = 2 \times 10^{-6}$ sec, the ellipse has nearly made its way back to equilibrium.

Figure 4 presents the time history of the probability density at the point $(X_1, X_2) = (5 \times 10^{-9}, 2.5 \times 10^{-9})$ m in position space. This figure represents the likelihood of seeing the column tip at this point in position space as a function of time. For $t \in [0, 4 \times 10^{-7}]$ sec, the probability density of seeing a column

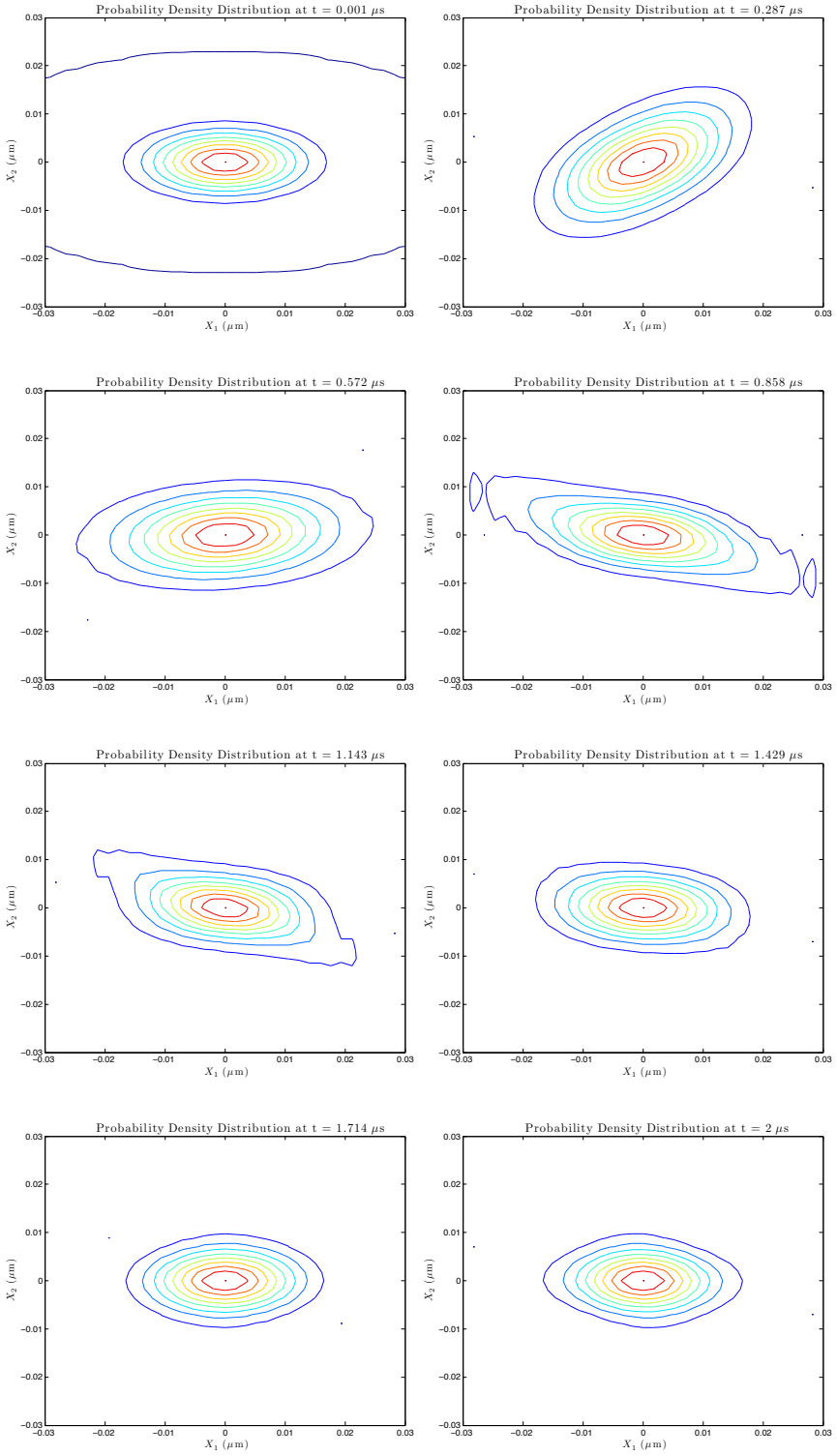

Figure 3: Contour snapshots of probability density distribution in position space at times t = 1×10^{-9}s, 2.87×10^{-7}s, 4×10^{-7}s, 5×10^{-7}s, 5.72×10^{-7}s, 1.143×10^{-6}s, 1.429×10^{-6}s, 2×10^{-6}s. Chronological order proceeds from left to right then top to bottom. $\dot{\theta}(t) = 1.1978\pi \times 10^{6}[H(t) - H(t - 4.0 \times 10^{-7})]$ Hz.

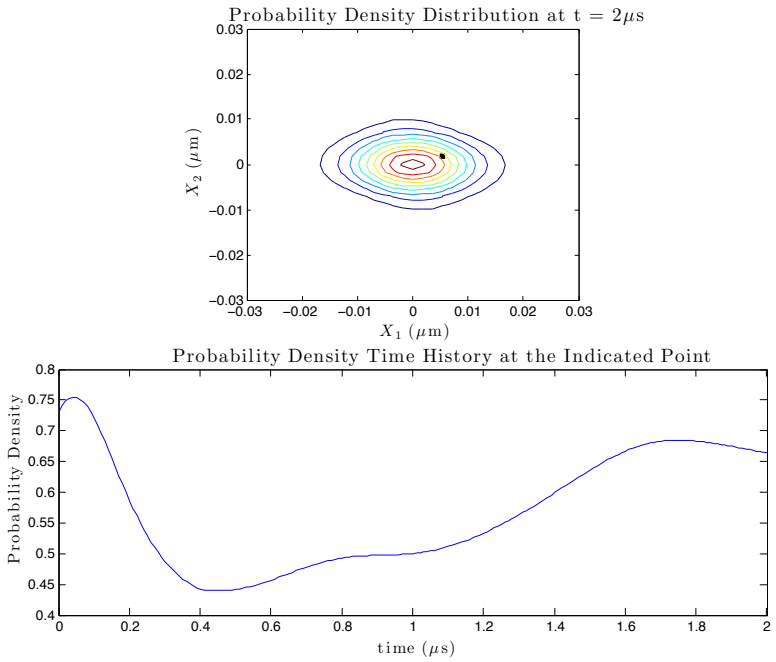

Figure 4: Probability density time history at the point $(X_1, X_2) = (5 \times 10^{-9}, 2.5 \times 10^{-9})m$ in position space. $\dot{\theta}(t) = 1.1978\pi \times 10^6[H(t) - H(t - 4.0 \times 10^{-7})]$ Hz.

tip at this point dramatically decreases. For $t \in [4 \times 10^{-7}, 2 \times 10^{-6}]$ sec, the probability density steadily rises. This is expected since in the first interval, the base plate is being rotated at $1.1978\pi \times 10^6$ Hz and in the second interval, the base is fixed. During the interval of rotation, the columns will experience large displacements resulting in a "spreading out" of the probability density (as argued above). During the interval of zero rotation, the collision term forces the system back to equilibrium, therefore increasing the probability density near the ellipse center.

6 Conclusion

There has been little work done on numerically integrating (1) due to the curse of dimensionality that quickly arises when one applies this equation to practical problems. This document presented a useful example where the dimensionality of the problem is small enough to feasibly solve. The results in this paper show promise for the future of this problem and some further work may include: 1) analytical expression for stability analysis, 2) tuning the parameters to elicit a more pronounced system response, and 3) determine a method for solving the desired inverse problem.

References

[1] R. Richtmyer and K.W. Morton. *Difference Methods for Initial-Value Problems.* Interscience Publishers, second edition, 1967.

[2] G. Zwas. On Two Step Lax-Wendroff Methods in Several Dimensions. *Numerische Mahematik*, 1971.